Transport Phenomena During Solidification Processing of Functionally Graded Composites by Sedimentation

J. W. Gao

C. Y. Wang
e-mail: cxw31@psu.edu

Department of Mechanical and Nuclear Engineering,
The Pennsylvania State University,
University Park, PA 16802

A combined experimental and numerical investigation of the solidification process during gravity casting of functionally graded materials (FGMs) is conducted. Focus is placed on understanding the interplay between the freezing front dynamics and particle transport during solidification. Transparent model experiments were performed in a rectangular ingot using pure water and succinonitrile (SCN) as the matrix and glass beads as the particle phase. The time evolutions of local particle volume fractions were measured in situ by bifurcated fiber optical probes working in the reflection mode. The effects of important processing parameters were explored. It is found that there exists a particle-free zone in the top portion of the solidified ingot, followed by a graded particle distribution region towards the bottom. Higher superheat results in slower solidification and hence a thicker particle-free zone and a higher particle concentration near the bottom. The higher initial particle volume fraction leads to a thinner particle-free region. Lower cooling temperatures suppress particle settling. A one-dimensional multiphase solidification model was also developed, and the model equations were solved numerically using a fixed-grid, finite-volume method. The model was then validated against the experimental results and subsequently used as a tool for efficient computational prototyping of an Al/SiC FGM. [DOI: 10.1115/1.1339976]

1 Introduction

The recently developed functionally graded materials (FGMs) have been highly considered as candidate materials for applications in severe environments confronting modern technologies. Among various FGMs, metal matrix composite FGMs are of great practical interest. Metal matrix composite FGMs feature gradual compositional variations from ceramic at one surface to metal at the other, leading to the unique advantages of a smooth transition in thermal stresses across the thickness and minimized stress concentration at the interface of dissimilar materials. As a result, such FGMs are rapidly finding applications in aggressive environments with steep temperature gradients such as turbine components and rocket nozzles.

Presently, there is no reliable and inexpensive way of fabricating FGMs that allows for bulk production of large parts. Current methods of fabrication include solidification processing, chemical vapor deposition, plasma spray and powder metallurgy techniques ([1]). Of these, perhaps the most economical and attractive processing route is gravity or centrifugal casting. The process involves the addition of a reinforcing particle phase to a liquid metal matrix and mixing them uniformly, followed by segregation of particles and liquid under gravity or in a centrifugal field to create a desired gradient in the particle concentration, and finally preservation of the spatially graded structure by solidification. Various FGMs such as metal-intermetallic compounds, metal-ceramics and metal alloy-ceramics have been successfully synthesized by this method ([2–4]).

A wealth of complex transport phenomena may occur in solidification processing of FGMs, including the transport of fluid, heat and solute, which governs the migration of particles in a liquid matrix, the interactions of particles with the advancing solidification front, and finally the incorporation of particles within the solidifying matrix. In order to create a desired particle distribution in the solidified part, the solidification time must be controlled such that it will be long enough to create the particle gradient but short enough to ''freeze'' the graded particle distribution in place. Therefore, it is of paramount importance to understand the solidification process with particle motion.

Particle sedimentation without solidification has been studied extensively in both fluidized bed and aqueous systems, but only a few investigations have addressed this problem in liquid metals. Hanumanth et al. [5] studied the sedimentation behavior of high volume fraction (as high as 0.30) of 90 μm diameter SiC particles in liquid aluminum using an electrical resistance probe to measure the in situ particle volume fraction. A multiphase hydrodynamic model was developed to describe the sedimentation. Using the same resistance probe, settling and clustering of 14 μm SiC particles in Al melts were monitored and analyzed by Irons and Owusu-Boahen [6]. From their analysis, the observed settling rates were consistent with that of 38 μm clusters containing ~42 percent particles by volume within the clusters. It was concluded that intense stirring prior to settling would result in smaller clusters.

Solidification of particle-reinforced metal-matrix composites (SiC particle in an aluminum alloy) was recently studied by Hanumanth and Irons [7] both numerically and experimentally. A one-dimensional enthalpy model was developed. In their model, particle velocity was simply estimated from the Richardson-Zaki hindered settling correlation ([8]), without solving the coupled momentum and continuity equations. This approach implies that the counter-current displacement flow of liquid due to particle sedimentation was not accounted for, which could lead to substantial overestimation of the particle phase velocity (i.e. by a factor of $1/1-\varepsilon_p$, where ε_p is the particle volume fraction). The mushy zone evolution was described using the Scheil equation. The effects of cooling rate and thermal conductivity of SiC particles were explored. It was proposed that the SiC particle thermal con-

Contributed by the Heat Transfer Division for publication in the JOURNAL OF HEAT TRANSFER. Manuscript received by the Heat Transfer Division February 29, 2000; revision received October 11, 2000. Associate Technical Editor: D. A. Kaminski.

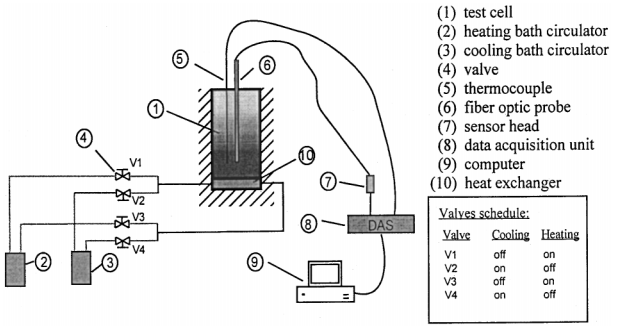

Fig. 1 Schematic of experimental setup

ductivity should be on the order of the single crystal value for accurate representation of cooling rates and particle settling, although very little settling was found to occur for the prescribed cooling condition. Feller and Beckermann [9] developed a multiphase model for the alloy solidification of metal-matrix particulate composites with convection. The Happel ([10]) hindered settling function was used. The model was applied to various one and two-dimensional Al-7 wt pct Si/SiC systems. Good agreement was found between the simulation and available experimental sedimentation results in A356 systems containing clustering and non-clustering SiC particles.

The previous studies focused mainly on the final distribution of particles, whereas virtually no information on the time evolution of the coupled solidification and sedimentation events was revealed. Therefore, detailed mechanisms for particle segregation in a solidifying matrix, which are of paramount importance for the design of FGMs, remain elusive. Also, limited experimental work in the past has not provided detailed data on time evolution of the particle concentration distribution during matrix solidification. The availability of these data during processing is necessary to rigorously validate any sophisticated model describing FGM solidification. The present work is thus aimed at studying the detailed solidification process during gravity casting of FGMs by means of in situ measurements of both temperature and particle volume fraction. Transparent model experiments were performed using pure substances as the matrix and glass beads as the particle phase. Local particle volume fractions were measured by fiber optic probes, making it possible to obtain the volume fraction changes with time during settling and solidification. Subsequently, a one-dimensional numerical model, derived from the general multiphase solidification model of Wang [11], was developed and validated against the experimental results. The validated code was used as a tool for ''computational prototyping'' of as-cast FGMs.

2 Experimental Setup and Procedures

The experimental setup is schematically shown in Fig. 1. The rectangular test cell consists of a stainless steel heat exchanger cold plate as the bottom wall, a Plexiglas top wall and center section. Cooling was accomplished by passing a mixture of ethylene glycol and water (1:1) through the heat exchanger.

The glass beads supplied by MO-SCI Corporation were used as the particle phase. The mean diameter of the particles was found to be 30 μm with a standard deviation of 9 μm. The matrix liquids were succinonitrile from Alfa Aesar (purity: 98^+ percent, melting temperature 58°C) and distilled water, respectively.

A. Temperature Measurement. Temperature measurements were performed using copper-constantan (type-T) thermocouples that were mounted through the top panel of the test cell. Modular plug-in thermocouples (Omega Model number TMQSS-020-6) were used, calibrated to an accuracy of ± 0.3°C. Four thermocouples were placed at different height in the test cell, with positioning uncertainty of ± 1 mm. Each experiment was repeated three times by varying the horizontal position of each thermocouple at fixed height. The maximum temperature difference along the horizontal plane was found to be 0.5°C.

B. Particle Volume Fraction Measurement. There are a number of techniques for the measurement of solid concentrations in multiphase flows ([12]). Among these techniques, fiber optic probes working in reflection mode are extensively used, especially for gas/solid flows in circulating fluidized beds. In the reflection mode, light is carried by the emitting fiber into a measuring volume and reflected back by the particles to the receiving fiber. Therefore, the reflection mode is especially suitable for measurements of dense suspensions.

Characteristics of Fiber Optical Probes. Plastic bifurcated fiber optic probes (model PBP26U) from Banner Engineering Corporation were used in this study. The probe has two parallel plastic optical fibers of 0.5 mm core size, bifurcated and shielded by annealed stainless steel. The probe was connected to an analog Umni-Beam sensor head (model OASBFP, Banner), which contains a light source (visible red $\lambda = 650$ nm) for the emitting fiber and a photodetector for the receiving fiber to convert the reflected light intensity to voltage signals. The time constant of the sensor is 2 ms, rendering the probes sufficiently fast for transient experiments. Subsequent signal sampling and processing were made by a PowerMac computer. More details can be found in Gao et al. [13].

Calibration. Each probe was calibrated before being used in the experiments. Detailed calibration procedures are described in Gao et al. [13]. The calibrations were first made in water/glass-bead suspensions. It was found that the measurement can be described by

$$\Delta U = U - U_0 = a\varepsilon_p^b, \tag{1}$$

where U is the output of the sensor at a particle volume fraction of ε_p, and U_0 represents the reading obtained in the same fluid without particles. This correlation is consistent with those shown by Hartge et al. [14] and Nieuwland et al. [12]. It is also found that the exponent b depends only on the properties of the particles and probes whereas the factor a depends on the carrier fluid (i.e., the liquid matrix here). Since the exponent b is independent of the type of fluids, the values of b determined in water/glass-bead suspension can be used in other glass-bead suspensions with transparent carrier fluids. This offers great advantages for the calibration of probes, especially for those carrier fluids that are solid at room temperature such as succinonitrile (SCN). Several suspensions of SCN/glass-bead with known particle volume fractions, namely 15 percent, 20 percent, and 40 percent, were used to obtain the numerical factors. These calibrated values along with complete calibration curves are given in detail in Gao et al. [13].

During the solidification and sedimentation experiments, the probes were inserted into the test cell through the top wall and were positioned by a scale, with positioning uncertainty of ± 1 mm.

C. Experimental Procedures. Suspensions were prepared by mixing particles with a liquid matrix. Before the experiments, the mixture was preheated to a certain superheat by pumping the working fluid from the heating circulator through the heat exchanger. At the desired temperature, the melt was stirred to form a homogenous suspension. At the same instant when stirring was stopped, the fiber optic probes and thermocouples were quickly inserted into the test cell. At this point, the coolant with preset temperature was run through the heat exchanger and the data acquisition system was initiated, with the sampling rate of 0.5 Hz for both temperature and particle volume fraction measurements.

Table 1 Thermophysical properties of succinonitrile/glass-bead

Quantity	Symbol	Value	Units	Reference
Liquid density	ρ_l	986.7	kg/m^3	Sekerka et al. (1995)
Solid density	ρ_s	986.7	kg/m^3	assumed
Particle density	ρ_p	2500	kg/m^3	MO-SCI Inc.
Liquid viscosity	μ_l	2.56×10^{-3}	kg/m s	Sekerka et al. (1995)
Liquid specific heat	C_{pl}	2000	J/kg K	Rubinstein and Glicksman (1991)
Solid specific heat	C_{ps}	1910	J/kg K	Rubinstein and Glicksman (1991)
Particle specific heat	C_{pp}	745	J/kg K	Incropera and DeWitt (1996)
Liquid thermal conductivity	k_l	0.223	W/m K	Sekerka et al. (1995)
Solid thermal conductivity	k_s	0.223	W/m K	Sekerka et al. (1995)
Particle thermal conductivity	k_p	1.40	W/m K	Incropera and DeWitt (1996)
Latent heat of fusion (pure SCN)	Δh	4.62×10^4	J/kg	Rubinstein and Glicksman (1991)
Melting temperature (pure SCN)	T_m	331.0	K	Rubinstein and Glicksman (1991)

3 Numerical Modeling

A. Model Formulation. A general multiphase modeling framework developed by Wang [11] is used to build the present model. The following assumptions are invoked:

1 One-dimensional planar solidification.

2 The model treats particles, liquid and forming solid as separate phases.

3 The motion of particles is slow and reaches the terminal velocity instantaneously. This assumption is appropriate due to the small size of the particles.

4 Local thermal equilibrium exists, which is justified by the typically large thermal conductivities of metals.

5 Particle pushing at the solid/liquid interface does not occur due to the relatively high advancing velocity of the solidification front in the present study as compared to the critical velocity for pushing, as shown by Gao et al. [13]. This fact is also well supported by our experimental observations.

6 The particles are rigid and spherical, and do not react chemically with the matrix.

7 Volume change during solidification is negligible.

8 All thermophysical properties are assumed to be constant as given in Tables 1 and 2.

With the preceding assumptions, a working model can be formulated from the general multiphase model as follows.

Table 2 Thermophysical properties of Al/SiC

Quantity	Symbol	Value	Units	Reference
Liquid density	ρ_l	2390	kg/m^3	Smithells (1976)
Solid density	ρ_s	2550	kg/m^3	Smithells (1976)
Particle density	ρ_p	3200	kg/m^3	Smithells (1976)
Liquid viscosity	μ_l	1.26×10^{-3}	kg/m s	Landolt and Börnstein (1965)
Liquid specific heat	C_{pl}	1079.5	J/kg K	Smithells (1976)
Solid specific heat	C_{ps}	1176.5	J/kg K	Smithells (1976)
Particle specific heat	C_{pp}	840	J/kg K	Smithells (1976)
Liquid thermal conductivity	k_l	95	W/m K	Smithells (1976)
Solid thermal conductivity	k_s	210	W/m K	Smithells (1976)
Particle thermal conductivity	k_p	16	W/m K	Stefanescu et al. (1988)
Latent heat of fusion (pure Al)	Δh	3.97×10^5	J/kg	Smithells (1976)
Melting temperature (puer Al)	T_m	933.6	K	Smithells (1976)

Mass Conservation Equations

$$\text{Particle:}\quad \frac{\partial}{\partial t}(\rho_p\varepsilon_p)+\frac{\partial}{\partial y}(\rho_p\varepsilon_p v_p)=0 \tag{2}$$

$$\text{Solid:}\quad \frac{\partial}{\partial t}(\rho_s\varepsilon_s)=\Gamma_s \tag{3}$$

$$\text{Liquid:}\quad \frac{\partial}{\partial t}(\rho_l\varepsilon_l)+\frac{\partial}{\partial y}(\rho_l\varepsilon_l v_l)=-\Gamma_s \tag{4}$$

Momentum Conservation Equations

$$\text{Particle:}\quad -\varepsilon_p\frac{\partial p}{\partial y}-\rho_p\varepsilon_p g+M_p^d=0 \tag{5}$$

$$\text{Liquid:}\quad -\varepsilon_l\frac{\partial p}{\partial y}-\rho_l\varepsilon_l g-M_p^d=0 \tag{6}$$

Energy Conservation Equation

$$\frac{\partial}{\partial t}[(\rho_s\varepsilon_s C_{ps}+\rho_p\varepsilon_p C_{pp}+\rho_l\varepsilon_l C_{pl})T]+\frac{\partial}{\partial y}[(\rho_p\varepsilon_p C_{pp}v_p+\rho_l\varepsilon_l C_{pl}v_l)T]=\frac{\partial}{\partial y}\left[(\varepsilon_s k_s+\varepsilon_p k_p+\varepsilon_l k_l)\frac{\partial T}{\partial y}\right]+\Gamma_s[\Delta h+(C_{ps}-C_{pl})T_m] \tag{7}$$

Boundary Conditions

$$y=0\quad T=T_w,\quad \frac{\partial\varepsilon_p}{\partial y}=\frac{\partial\varepsilon_l}{\partial y}=0,\quad v_p=v_l=0$$

$$y=l\quad \frac{\partial T}{\partial y}=0,\quad \frac{\partial\varepsilon_p}{\partial y}=\frac{\partial\varepsilon_l}{\partial y}=0,\quad v_p=v_l=0$$

Initial Conditions

$$T=T_i\quad \varepsilon_p=\varepsilon_{pi}\quad \varepsilon_s=\varepsilon_l=0\quad \text{at } t=0$$

Constitutive Equation

$$\varepsilon_p+\varepsilon_s+\varepsilon_l=1 \tag{8}$$

Following Wang [11], the liquid-particle drag term M_p^d in a multiparticle system can be modeled as

$$M_p^d=\frac{18(1-\varepsilon_l)\mu_l C_\varepsilon}{d^2}\varepsilon_l^2(v_l-v_p), \tag{9}$$

where the settling ratio for a multiple particle system, C_ε, accounts for all departures from the idealized single solid sphere settling as described by Stokes law. In this study, the well established hindered settling function of Richardson and Zaki [8] was utilized,

$$C_\varepsilon=(1-\varepsilon_p)^{-4.65}. \tag{10}$$

Further manipulation of momentum Eqs. (5) and (6) by incorporating Eqs. (2)–(4) and (9) gives:

$$v_p=-\frac{(\rho_p-\rho_l)\varepsilon_p g d^2}{18\mu_l(1-\varepsilon_l)C_\varepsilon(\varepsilon_p+\varepsilon_l)^2}\quad v_l=-\frac{\varepsilon_p v_p}{\varepsilon_l}. \tag{11}$$

Equation (11) is valid in the free particle regime, whereas for the packed bed regime both v_p and v_l are set to be zero.

B. Numerical Procedures. The conservation equations are solved simultaneously using a fixed-grid, single-domain numerical solution procedure. A fully-implicit, control-volume based finite difference method is utilized to discretize the conservation equations (2), (3), and (7), with the finite-difference coefficients

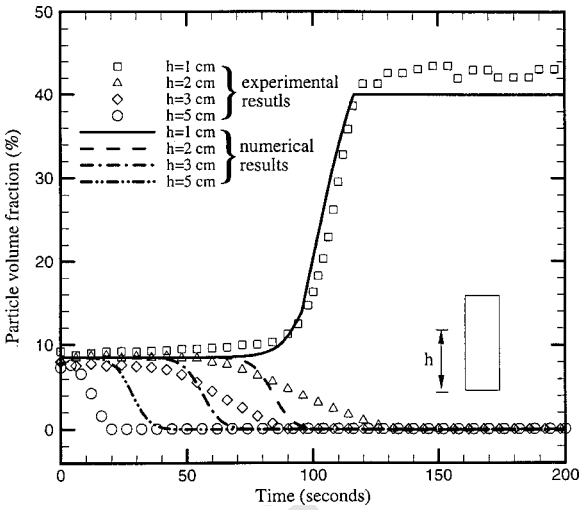

Fig. 2 Sedimentation curve for a water/glass-bead system (ε_{pi}=8.5 percent at room temperature)

evaluated by the upwind scheme. The discretized equations are solved iteratively. The detailed procedures can be found in the literature ([13]).

Stringent numerical tests were performed to ensure that solutions were independent of the grid size and time step. For a typical water/glass-bead solidification system, the maximum difference in temperature and particle volume fraction is less than 0.02°C and 0.1 percent, respectively for a grid size containing 40 to 150 control volumes. Virtually no difference was found in the results for time steps ranging from 0.02 s to 5 s. It was found that a grid containing 60 control volumes in the *y*-direction with a single control volume in the *x*-direction provides sufficient spatial resolution. Previous experience has also shown that such a grid is able to capture all dynamic solidification features at a reasonable computational cost ([11]). A time step of 0.5 s was utilized for all simulations reported in the following.

4 Results and Discussion

A. Model Validation

Sedimentation. A mixture of water and 8.5 percent volume fraction of glass beads was poured into the test cell to produce a melt height of 6 cm. The sedimentation results are plotted in Fig. 2. It can be seen that in general, the model prediction agrees well with the experimental results, which show the characteristics of one-dimensional batch sedimentation, as depicted in the literature ([7,15]). That is, a particle-free zone starts to form from the top and a layer of sediment on the bottom; in the middle portion of the cell, the particle volume fraction remains the initial particle volume fraction for a period of time and then starts to monotonically decrease to zero. Note that within the sediment bed (i.e., 1 cm away from the bottom), the particle volume fraction approaches 40 percent, lower than the random close packing factor of 60 percent. This can be attributed to the fact that the particles may form clusters during sedimentation, resulting in a loosely packed sediment at the bottom. This packing limit will be utilized in all of the numerical simulations. The experimental result for the location 5 cm away from the bottom exhibits faster settling than the model prediction, which may be due to the fact that the vortex motion of the suspension during the stirring persists and hence expedites the settling. This effect is most pronounced on the settling of particles at the top, where the particle-free zone forms before the vortex motion dies out. It is also interesting to notice more gradual decreases of the particle volume fraction in the experimental sedimentation curves at positions 2 and 3 cm away from the bottom. This may be attributed to the particle size distribution of the glass beads used.

It should be pointed out that there are a number of hindered settling functions in the literature ([16]), obtained mainly from aqueous or gas/solid systems. Among those relations, the Happel and Richardson-Zaki relations have been used most widely. Preliminary simulations showed that if the Happel hindering function was applied in the present model, the predicted settling rate is about half of that with the Richardson-Zaki function, i.e., Eq. (10). Feller and Beckermann [9] used the Happel relation in their model and discussed their results in relation to the study of Hanumanth et al. [5], in which the Richardson-Zaki's function was applied. They concluded that the Richardson-Zaki relation overestimates the settling rate. They attributed the good agreement between the experimental and modeling results in the study of Hanumanth et al. [5] to a larger liquid melt viscosity used. The present study, however, indicates that the Richardson-Zaki function gives more realistic predictions, which is consistent with numerous studies in the literature for aqueous and gas/solid systems ([16]). Since the current study was performed for water, whose thermophysical properties are well documented in the literature and can be evaluated accurately, the viscosity is unlikely a factor that affects the above conclusion.

Solidification With Particle Sedimentation. Experiments and simulations were performed to validate the model in dealing with combined solidification and particle settling. For each simulation, the measured wall temperature from the experiments was fitted to a polynomial function, namely $T_w = f(t)$, to give temperature boundary conditions for the energy equation.

The mixture used in the preceding sedimentation experiment was solidified from an initial temperature of 23°C. The cooling curves and time evolution of particle concentrations are plotted in Figs. 3(*a*) and 3(*b*). Good agreement between the experiment and simulation was achieved. It can be seen that due to the large latent heat of water, the solidification is fairly slow and therefore the curves for the particle volume fraction are very similar to those in the pure sedimentation case shown in Fig. 2.

With the same initial temperature, a water/glass-bead suspension with an initial particle volume fraction of 20 percent was solidified. The results are plotted in Figs. 4(*a*) and 4(*b*). The model prediction is in good agreement with the experiment.

One interesting feature is that the wall temperature experiences an increase around 150 seconds into the experiment. This is found in cooling curves for both cases (see Figs. 3(*a*) and 4(*a*)), and can be explained by the fact that freezing occurred at this time instant, releasing a large amount of latent heat and therefore increasing the local temperature. This phenomenon was not observed in the solidification of the SCN/glass-bead system probably due to the much smaller latent heat of succinonitrile.

B. SCN/Glass-Bead Systems. Due to its high specific heat and low freezing temperature, the water/glass-bead system does not allow much room for the investigation of various processing conditions. Therefore, in the subsequent experimental studies, a SCN/glass-bead system was investigated.

The suspensions were prepared by mixing prescribed volume fractions of glass beads with SCN and forming a melt height of 6.35 cm for all experiments. The experimental conditions are summarized in Table 3.

Base Case. Figures 5(*a*) and 5(*b*) show the results for a base case having a 20 percent volume fraction of particles, a cooling temperature of −10°C, and an initial temperature of 63°C. Comparing the experimental and numerical results, reasonable agreement was found for the cooling curve, while agreement for the time evolutions of the particle concentration is only fair. The discrepancy may be attributed to the purity of SCN used in this study, namely 98^+ percent. Under certain cooling conditions, den-

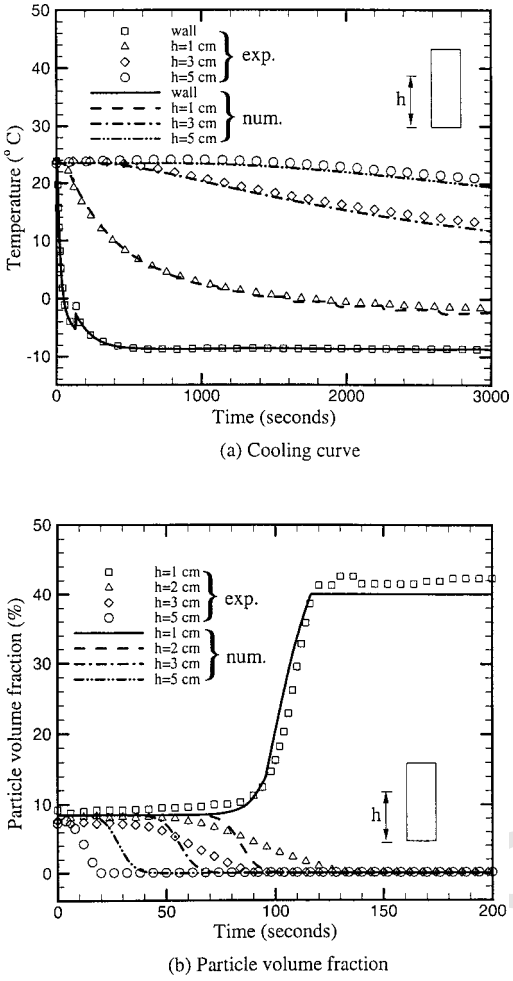

Fig. 3 Solidification of a water/glass-bead suspension (ε_{pi} = 8.5 percent, T_i = 23°C): (*a*) cooling curve; (*b*) time evolution of particle volume fraction

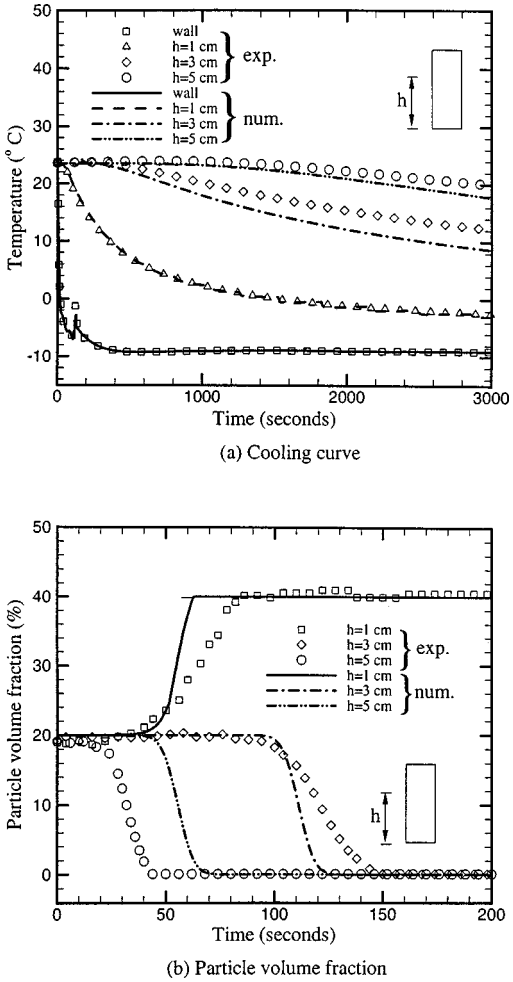

Fig. 4 Solidification of a water/glass-bead suspension (ε_{pi} = 20 percent, T_i = 23°C): (*a*) cooling curve; (*b*) time evolution of particle volume fraction

dritic microstructures were observed that would affect the measurement of particle volume fractions, especially in the solidifying region.

The final particle concentration distributions measured and predicted for the baseline case are shown in Fig. 6(*a*). Upon cooling, the melt close to the wall solidified first so that the particle volume fraction was fixed approximately at its initial value. This occurs relatively quickly, as is shown by the cooling curve for the first thermocouple (at the wall). For subsequent points away from the wall, the particle volume fraction increases due to settling from above before solidification, leading to a higher particle volume fraction. Solidification, however, interrupts the settling process: when the solidification front passes through a certain control volume, it freezes the local particle concentration in place and stops the particle flow from the above. This results in an increasing particle concentration at the location right above it since the control volume at this location only receives particles from its upper neighbor. In the meantime, when moving upward, the solidification front becomes slower, allowing more time for particles to settle. This trend develops as the solidification and settling progresses, resulting in a graded layer of about 7 mm thick from the bottom, with an almost linearly increasing particle concentration across the layer (see Fig. 6). Above this layer, solidification was not fast enough, hence a layer of packed-bed particle volume fraction was formed, followed by a particle-free zone on top of it.

Parametric Study. In this section, effects of different parameters on the final particle concentration distribution are examined.

Figure 6(*a*) also summarizes the effect of increasing superheat of the melt. It is indicated that increasing the superheat (from 5°C to 10°C) slows down the solidification allowing for more particles to settle before freezing occurs. Therefore the final particle distribution is slightly higher throughout most of the test cell with more of the cell being occupied by pure succinonitrile for Case 2.

Figure 6(*b*) shows that increasing the temperature of the bottom cold wall, as expected, produces a slightly thinner graded layer. The higher cooling temperature causes slower solidification, and therefore the particles have more time to settle before solidification, resulting in a thinner graded layer with higher local particle concentration as compared to the corresponding locations in the base case.

Table 3 Experimental conditions for SCN/glass-bead systems

Case #	Initial Particle Volume Fraction (%)	Superheat ΔT (K)	Cooling Temperature (°C)
1 (baseline case)	20	5	-10
2	20	10	-10
3	20	5	5
4	15	5	-10

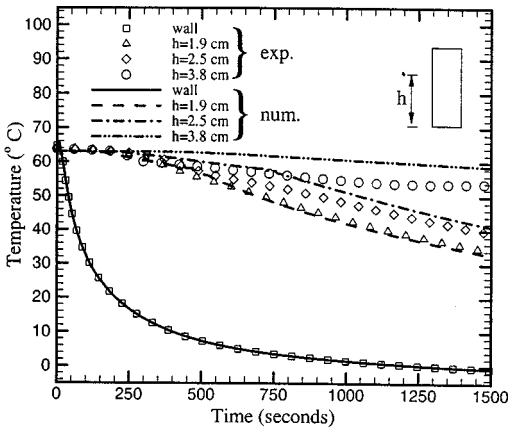

(a) Cooling curve

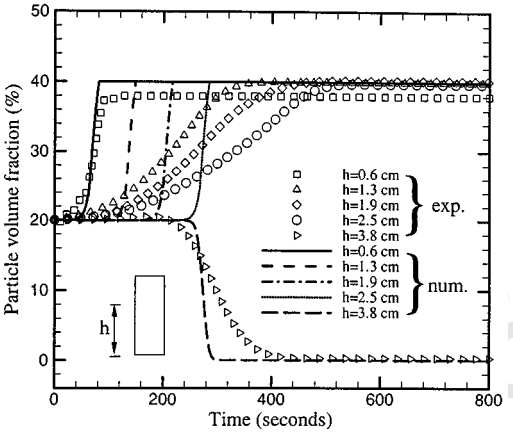

(b) Particle volume fraction

Fig. 5 Solidification of a SCN/glass-bead suspension (ε_{pi} = 20 percent, T_i = 63°C): (*a*) cooling curve; (*b*) time evolution of particle volume fraction

The effects of the initial particle concentration are much more pronounced, as indicated in Fig. 6(*c*). When the initial particle volume fraction is decreased from 20 percent to 15 percent, two of the probes show zero readings, indicating a larger particle-free region at the top. A thicker gradient layer is formed but with generally lower particle concentrations. This is due to the fact that there are fewer particles in the system, requiring a longer time for particles to settle before they become packed.

FGM Solidification Mechanisms. From the above analysis, two factors can be identified to be responsible for creation of the graded structure in a solidified FGM, namely, particle migration and solidification. Particle migration segregates the particles from the liquid melt and thus creates a gradient in their volume fraction. Solidification interrupts the particle migration and alters the segregation process, in such a way that it ''freezes'' the local particle concentration in place and alters the particle migration in the non-solidified regions. In view of the interplay between the two factors, one can tailor a gradient in an FGM by controlling the various processing conditions.

C. Solidification of Al-SiC FGMs. The validated code was applied to simulate the casting of Al-SiC FGMs from a melt 6 cm in height, with the bottom chill surface maintained at a constant temperature. The packed particle volume fraction was set to be 40 percent. Although this value may vary in reality, depending on the degree of particle clustering, the general conclusions are still applicable.

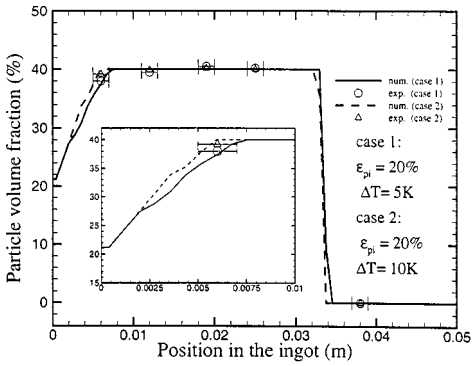

(a) Comparison for different superheats

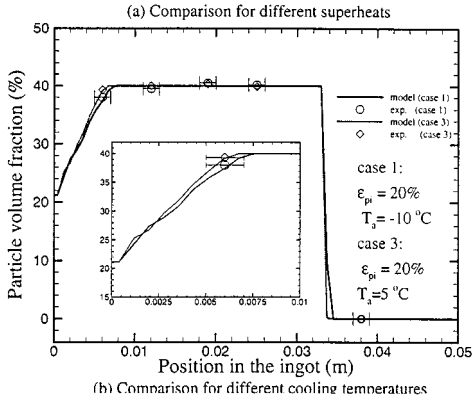

(b) Comparison for different cooling temperatures

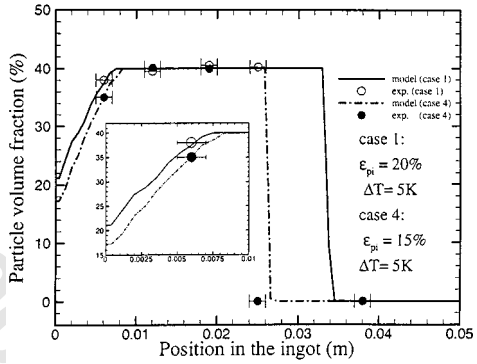

(c) Comparison for different initial particle concentrations

Fig. 6 Particle concentration distribution in a solidified SCN/glass-bead system under different processing conditions

Figure 7(*a*) explores the effect of cooling temperatures for a melt initially containing 20 percent SiC particles of 20 microns. It can be seen that a higher cooling temperature will allow particles to settle, and hence generate a certain gradient in the solidified part. Low cooling temperature freezes the melt quickly due to the large thermal conductivity of aluminum and therefore the particles do not have time to segregate, leading to a nearly homogeneous particle distribution.

Melts containing three different particle sizes are solidified, as shown in Figure 7(*b*). Larger particles settle faster and thus form a packed bed more easily, which is the case for 40 μm particles where a gradient is confined within a 2 cm region towards the bottom with a packed bed of about 1.5 cm in thickness followed. For particles of 10 μm, however, the sedimentation is too slow and the final particle concentration is almost uniform throughout the ingot.

The initial particle volume fraction has a significant effect on the final particle distribution, especially for a larger particle size like 40 μm, as indicated in Fig. 7(*c*). A gradient is formed from the bottom of the ingot in all three cases. The initial particle concentration of 10 percent gives the thickest gradient region and

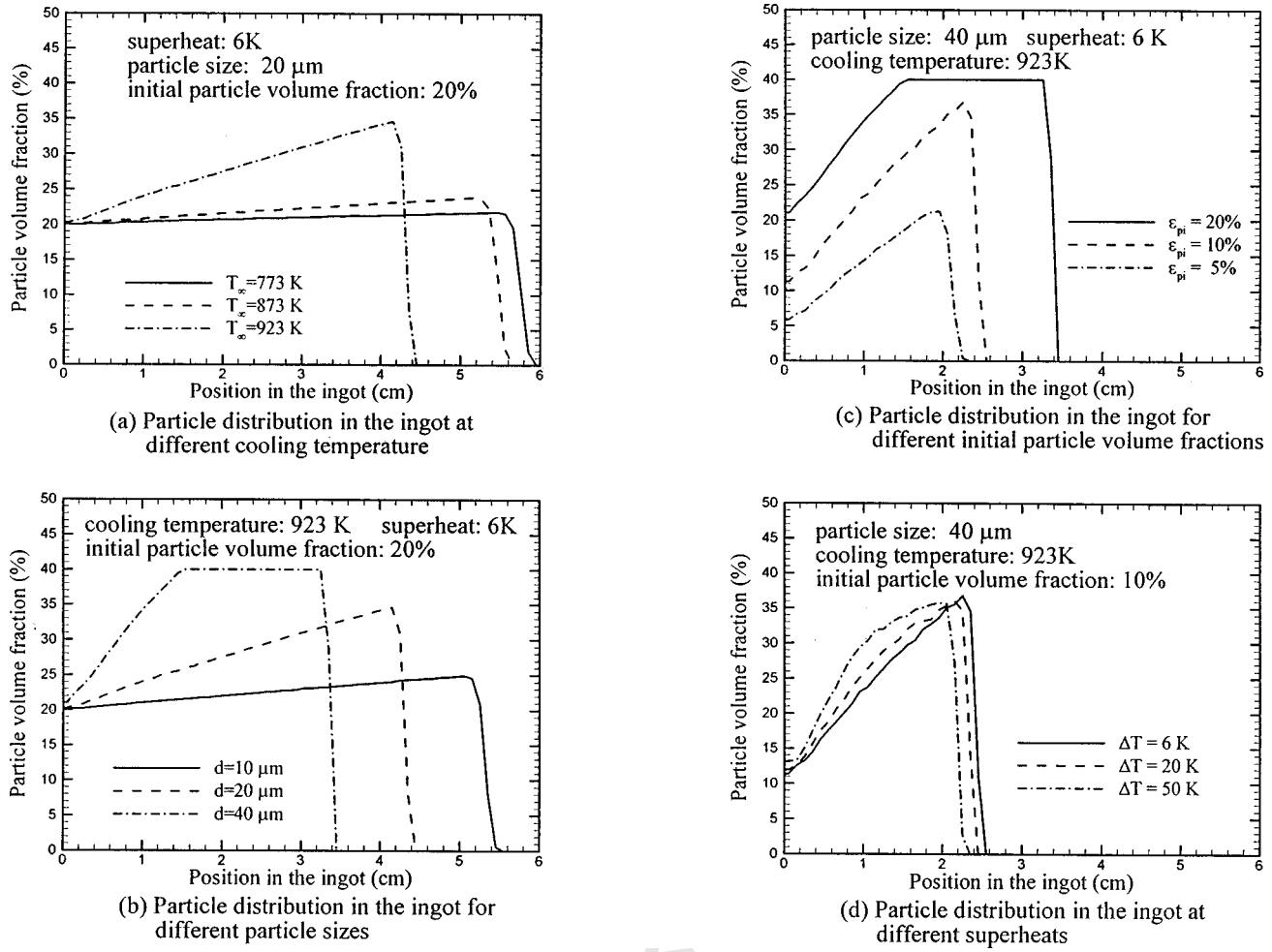

Fig. 7 Particle concentration distribution in a solidified Al/SiC composite under different processing conditions

the steepest gradient. 20 percent initial particle concentration results in a thick packed bed region whereas the 5 percent case simply does not have enough particles to generate a thick gradient layer. Therefore, in the casting practice, there exists an optimized initial particle volume fraction at a specific particle size for a desired particle gradient.

The effect of superheat, however, is not pronounced as can be seen from Fig. 7(*d*), which may be attributed to the large thermal conductivity of aluminum, allowing the superheat to be dissipated quickly upon cooling. A higher superheat allows slightly more time for particles to settle and hence a thinner gradient layer and a higher particle concentration at the same position in the graded zone.

The simulations confirm that the generation of a particle concentration gradient is determined by the competition between the rates of particle sedimentation and matrix solidification. It should be pointed out that in this study the final profiles of particle concentration do not vary monotonically across the entire part. Instead, there exists a layer of increasing particle volume fraction from the initial concentration to the packing limit, followed by a particle-free region on top of it (see Figs. 6 and 7). This is due to the fact that cooling starts instantaneously with the settling process, resulting in a particle concentration being close to the initial value at the cold surface. In order to obtain a monotonically varying particle distribution in the finally solidified part, one could delay the cooling until the maximum particle concentration (i.e., a packed bed) forms at the bottom followed by a layer of decreasing particle concentration upwards. The multiphase model developed in this study can be applied to design such a delayed cooling scheme to achieve the desired gradient. Research is underway to find an optimized set of processing conditions using an inverse problem design methodology.

5 Conclusions

Both experimental and numerical studies have been carried out for solidification of FGMs. Key conclusions from this study are as follows:

1 Fiber optic probes working in the reflection mode were successfully applied to the in situ measurement of particle volume fraction.

2 The experiments were performed to provide benchmark data on the time evolution of the particle distribution during solidification processing as well as to investigate effects of various processing parameters. The interplay between solidification and particle transport was elucidated in relation to creation of gradient structures in FGMs.

3 The multiphase solidification model developed in this study was extensively validated against the experimental results and generally good agreement was found. Simulations for the Al/SiC FGMs indicated that by optimizing the processing conditions, such as particle size, initial particle concentration, cooling rate and superheat, one can engineer a desired gradient in the solidified part.

Future work will focus on other modes of the interactions between particles and the solidification front, e.g., particle pushing and clustering. The model can also be extended to design centrifu-

gally cast FGMs. Research is also underway to investigate multi-dimensional solidification with melt convection in the presence of particles ([17–23]).

Acknowledgment

This work was supported by National Science Foundation under Grant No. CTS-9733662.

Nomenclature

a = coefficient in Eq. (1)
b = exponent in Eq. (1)
C_p = specific heat, J/kg-K
C_ε = hindered settling function
d = diameter of particles, μm
g = gravitational acceleration, m/s^2
k = thermal conductivity, W/mK
l = height of the suspension, m
M_p^d = solid/liquid drag per unit volume, N/m^3
p = pressure, N/m^2
T = absolute temperature, K
T_m = melting temperature, K
T_w = wall temperature, K
t = time, s
U = sensor output, V
v = velocity component in y-direction, m/s
y = y-coordinate in Cartesian system, m

Greek Symbols

ε_k = volume fraction of phase k, $[-]$
ε_{pi} = initial particle volume fraction, $[-]$
Γ_s = phase change rate, kg/m^3-s
μ = dynamic viscosity, N·s/m
ρ = density, kg/m^3
Δh = latent heat of fusion, J/kg

Subscripts

i = initial condition
l = liquid phase
p = particle phase
s = solid phase

References

[1] Mortensen, A., and Suresh, S., 1995, ''Functionally Graded Metals and Metal-Ceramic Composites: Part 1 Processing,'' Int. Mater. Rev., **40**, No. 6, pp. 239–259.
[2] Lajoye, L., and Suéry, M., 1988, ''Modelling of Particle Segregation During Centrifugal Casting of Al-Matrix Composites,'' in *Cast Reinforced Metal Composites*, S. G. Fishman and A. K. Dhingra, Eds., ASM, Materials Park, OH, pp. 15–20.
[3] Fukui, Y., Takashima, K., and Photon, C. B., 1994, ''Measurement of Young's Modulus and Internal Friction of an In Situ Al-Al_3Ni Functionally Gradient Material,'' J. Mater. Sci., **29**, pp. 2281–2288.
[4] Fukui, Y., and Watanabe, Y., 1996, ''Analysis of Thermal Residual Stress in a Thick-Walled Ring of Duralcan-Base Al-SiC Functionally Graded Material,'' Metall. Trans. A, **27A**, pp. 4145–4151.
[5] Hanumanth, G. S., Irons, G. A., and Lafreniere, S., 1992, ''Particle Sedimentation during Processing of Liquid Metal-Matrix Composites,'' Metall. Trans., **23B**, pp. 753–762.
[6] Irons, G. A., and Owusu-Boahen, K., 1995, ''Settling and Clustering of Silicon Carbide Particles in Aluminum Metal Matrix Composites,'' Metall. Trans. B, **26B**, pp. 981–989.
[7] Hanumanth, G. S., and Irons, G. A., 1996, ''Solidification of Particle-Reinforced Metal-Matrix Composites,'' Metall. Trans. B, **27B**, pp. 663–671.
[8] Richardson, J. R., and Zaki, W. N., 1954, ''Sedimentation and Fluidization: I,'' Trans. Inst. Chem. Eng., **32**, pp. 35–53.
[9] Feller, R. J., and Beckermann, C., 1996, ''Modeling of Solidification of Metal-Matrix Particulate Composites with Convection,'' Metall. Trans. B, **28B**, pp. 1165–1183.
[10] Happel, J., 1958, ''Viscous Flow in Multiparticle Systems: Slow Motion of Fluids Relative to Beds of Spherical Particles,'' AIChE J., **4**, pp. 197–201.
[11] Wang, C. Y., 1994, ''Multi-Scale/-Phase Modeling of Dendritic Alloy Solidification,'' Ph.D. thesis, University of Iowa, Iowa City, IA.
[12] Nieuwland, J. J., Meijer, R., Kuipers, J. A. M., and Swaaij, W. P. M., 1996, ''Measurements of Solids Concentration and Axial Solids Velocity in Gas-Solid Two-Phase Flows,'' Powder Technol., **87**, pp. 127–139.
[13] Gao, J. W., White, S. J., and Wang, C. Y., 1999, ''Solidification Processing of Functionally Graded Materials by Sedimentation,'' in *Proc. of IMECE 99*, ASME, Nashville, TN.
[14] Hartge, E. U., Rensner, D., and Werther, J., 1988, ''Solids Concentration and Velocity Patterns in Circulating Fluidized Beds,'' *Proceedings from the 2nd International Conference on Circulating Fluidized Bed Technology*, Basu, J., and Large, J. F., Eds., Pergamon, Oxford, pp. 165–180.
[15] Gidspow, D., 1994, *Multiphase Flow and Fluidization: Continuum and Kinetic Theory Descriptions*, Academic Press, San Diego, CA.
[16] Davis, R. H., 1996, ''Velocities of Sedimenting Particles in Suspensions,'' *Sedimentation of Small Particles in a Viscous Fluid*, E. M. Troy, ed., Computational Mechanics Publications, UK, pp. 161–198.
[17] Incropera, F. P., and DeWitt, D. P., 1996, *Fundamentals of Heat and Mass Transfer*, 4th Ed., Wiley, New York.
[18] Landolt, H., and Börnstein, R., 1965, *Zahlenwerte und Funkt.*, Springer-Verlag, Berlin, Teil 2, Band IV.
[19] Rubinstein, E. R., and Glicksman, M. E., 1991, ''Dendritic Growth Kinetics and Structure II. Camphene,'' J. Cryst. Growth, **112**, pp. 97–110.
[20] Sekerka, R. F., Coriell, S. R., and McFadden, G. B., 1995, ''Stagnant Film Model of the Effect of Natural Convection on the Dendrite Operating State,'' J. Cryst. Growth, **154**, pp. 370–376.
[21] Smithells, C. J., 1976, *Metals Reference Book*, Butterworth and Co., London.
[22] Stefanescu, D. M., Dhindaw, B. K., Kacar, S. A., and Moitra, A., 1988, ''Behavior of Ceramic Particles at the Solid-Liquid Metal Interface in Metal Matrix Composites,'' Metall. Trans. A, **19A**, pp. 2847–2855.
[23] Voller, V. R., 1990, ''Fast Implicit Finite-Difference Method for the Analysis of Phase Change Problems,'' Numer. Heat Transfer, Part B, **17**, pp. 155–169.